Effects of field annealing on MnN/CoFeB exchange bias systems

P. Quarterman,[1,*] I. Hallsteinsen,[2,3] M. Dunz,[4] M. Meinert,[4] E. Arenholz,[2,5] J. A. Borchers,[1] and A. J. Grutter[1]
[1]*NIST Center for Neutron Research, National Institute of Standards and Technology, Gaithersburg, Maryland 20899, USA*
[2]*Advanced Light Source, Lawrence Berkeley National Laboratory, Berkeley, California 94720, USA*
[3]*Department of Electronic systems, Norwegian University of Science and Technology – NTNU, 7491 Trondheim, Norway*
[4]*Center for Spinelectronic Materials and Devices, Department of Physics, Bielefeld University, D-33501 Bielefeld, Germany*
[5]*Cornell High Energy Synchrotron Source, Cornell University, Ithaca, New York 14853, USA*

(Received 1 April 2019; revised manuscript received 22 May 2019; published 24 June 2019)

We report the effects of nitrogen diffusion on exchange bias in MnN/CoFeB heterostructures as a function of MnN thickness and field-annealing temperature. We find that competing effects occur in which high-temperature annealing enhances exchange bias in heterostructures with thick MnN through improved crystallinity, but in thinner samples this annealing ultimately eliminates the exchange bias due to nitrogen deficiency. Using polarized neutron reflectometry and magnetic x-ray spectroscopy, we directly observe increasing amounts of nitrogen migration from MnN into the underlying Ta seed layer with increased annealing temperature. In heterostructures with thin MnN layers, the resulting nitrogen deficiency becomes significant enough to alter the antiferromagnetic state before the Ta seed layer is nitrogen saturated. Furthermore, we observe intermixing at the MnN/CoFeB interface which is attributed to the nitrogen deficiency creating vacancies in the MnN layer after annealing in a field. This intermixing of Mn with Co and Fe is not believed to be the cause for loss of exchange bias when the MnN layer is too thin but is instead a secondary effect due to increased vacancies after nitrogen migration.

DOI: 10.1103/PhysRevMaterials.3.064413

I. INTRODUCTION

Spintronic memories, which rely on the magnetic tunnel junction (MTJ) as a fundamental building block, have garnered significant interest due to their potential applications in low-power nonvolatile memory [1–4]. In a typical MTJ, one of the ferromagnetic layers is used as a reference by pinning the magnetization direction using the exchange bias effect via an adjacent antiferromagnet [5]. For this pinned magnetization to serve as an effective reference layer, the antiferromagnetic layer must generate a large bias field with respect to the switching fields of the ferromagnetic layers and remain stable through device operation temperatures. Since traditional antiferromagnetic materials, such as IrMn and PtMn, contain expensive heavy-metal elements, antiferromagnetic alternatives without these materials are highly desirable for MTJ devices.

Recently, MnN has been investigated as a promising antiferromagnetic material for use in MTJs [6–9]. The θ phase of MnN is a tetragonal variation of the NaCl structure with bulk lattice parameters $a = b = 4.256$ Å, $c = 4.189$ Å at room temperature and has a Néel temperature of approximately 660 K [10–13]. Previous reports on polycrystalline MnN/CoFe structures show an exchange bias field of 180 mT, a blocking temperature of 453 K, and an interfacial exchange energy of $J_{\text{eff}} = 0.41\ \text{mJ/m}^2$ [6]. More recently, Dunz *et al.* have shown that high-temperature annealing can enhance the exchange bias field to greater than 200 mT [8]. However, the optimal field-annealing temperature depends strongly on the MnN thickness, and when the MnN thickness is below a critical thickness the high-temperature annealing process destroys the exchange bias effect. In this work, it was postulated that nitrogen diffusion from the MnN into underlying Ta seed layers is the cause, and Auger depth profiling showed that annealing does indeed lead to nitrogen migration. However, since Auger electron spectroscopy (AES) analysis is sensitive only to the structural depth profile, it does not provide insight into how nitrogen diffusion affects the magnetic properties and cannot explain the thickness dependence.

In this work, we use polarized neutron reflectometry (PNR) and x-ray magnetic circular dichroism (XMCD) to develop a comprehensive understanding of the structural and magnetic properties in samples with varied annealing temperature and MnN thickness. We demonstrate that the MnN layer must be sufficiently thick in comparison to the underlying Ta seed layer in order to maintain a robust exchange bias at high annealing temperatures. If the MnN layer is too thin relative to the Ta layer, then the MnN will become heavily nitrogen deficient before the Ta layer is saturated. This deficiency leads to interdiffusion with the ferromagnetic layer and suppression of the MnN antiferromagnetic order at the interface, causing the desired exchange bias effect to disappear.

II. EXPERIMENTAL METHODS

Thin-film samples of Ta(10)/MnN(t_{MnN})/CoFeB(t_{CoFeB})/TaO_x(2.5), where the nominal thicknesses are denoted in nanometers and $t_{\text{MnN}} = 30$ and 48 nm and $t_{\text{CoFeB}} = 1.6$ and 7 nm, were grown on thermally oxidized Si/SiO_2 ($t_{\text{SiO2}} = 50$ nm) substrates using magnetron sputtering at

*patrick.quarterman@nist.gov

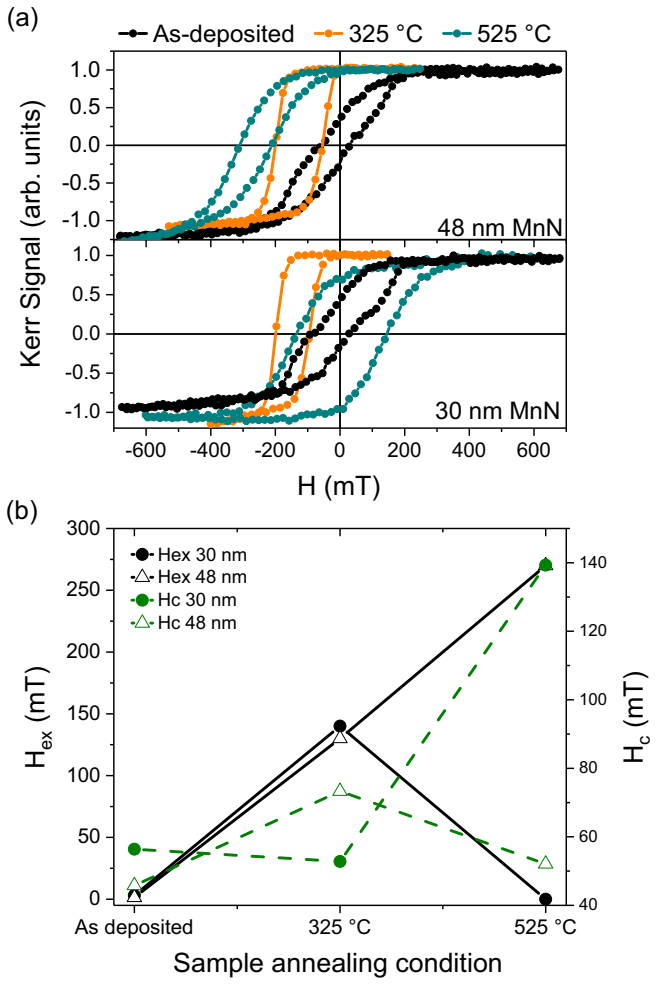

FIG. 1. (a) Normalized MOKE measured with field applied along the in-plane field-annealing axis for 1.6 nm CoFeB on 48 nm (top) and 30 nm (bottom) MnN. (b) Exchange bias field (black, solid) and coercive field (green, dashed) for the 30 nm (solid) and 48 nm (open) MnN samples with 1.6 nm CoFeB.

room temperature. The MnN layer was grown under reactive conditions using a Mn target and a Ar:N_2 gas ratio of 1:1. Exchange bias was set in the samples by postannealing under vacuum for 15 min, followed by field cooling at 650 mT along a direction parallel to the sample plane. We examined samples as deposited (non-field-annealed) and after field annealing at 325 and 525 °C. The crystallographic properties of MnN were probed using wide-angle x-ray diffraction (XRD) shown in Supplemental Material Fig. 1 [14]. The magnetization (M) as a function of applied field (H) was characterized using the longitudinal magneto-optical Kerr effect (MOKE). To probe the depth dependence of the nuclear structure and in-plane component of the magnetization, we measured PNR using the Polarized Beam Reflectometer instrument at the National Institute of Standards and Technology Center for Neutron Research. The incident neutron spins were polarized parallel or antiparallel to H, and reflectivity was measured in the non-spin-flip cross sections (R^{++} and R^{--}) as a function of the momentum transfer (Q) normal to the film surface. Measurements were collected at room temperature in a saturating magnetic field of 700 mT applied along the field-annealing direction. PNR data were reduced and modeled using the REDUCTUS and REFL1D software packages [15,16]. X-ray absorption spectra (XAS) were measured with circularly polarized x-rays and the XMCD spectra obtained as the difference between the XAS with antiparallel and parallel orientation of magnetization and photon helicity. All spectra were measured in total-electron yield (TEY) mode on the L_2 and L_3 edges for Fe, Co, and Mn, using beamline 4.0.2 at the Advanced Light Source. The samples were measured in the grazing incidence condition (30° from the sample plane) at room temperature and switching the magnetic field between ±0.3 T.

III. RESULTS

MOKE measurements for $t_{CoFeB} = 1.6$ nm and both MnN thicknesses are shown in Fig. 1(a). The substrate background was removed by subtracting a linear fit to the positive high-field data. At the corresponding high negative field region, the magnetization does not completely saturate, which may be indicative of an uncompensated, pinned moment [5]. The 30 nm MnN sample shows an exchange bias field (H_{ex}) of 140 mT after 325 °C field annealing, but the exchange bias disappeared after field annealing at 525 °C. A similar drop in H_B was observed in thinner MnN layers at high annealing temperature. The 48 nm MnN sample, however, shows H_{ex} increased from 130 mT at 325 °C to 270 mT at 525 °C. Additionally, the 30 nm MnN sample showed an increased coercive field (H_c) from 57 to 135 mT after annealing at 525 °C, while the 48 nm MnN sample exhibited no noticeable increase for H_c. The exchange bias field and coercivity as a function of annealing temperature are plotted in Fig. 1(b). Previously, Ta/MnN/CoFe structures have been studied with AES and MOKE [8]. In these reports, AES suggested nitrogen diffusion into Ta in all samples considered upon annealing.

To further understand the role of annealing and nitrogen diffusion, PNR has been measured on the 7 nm CoFeB set of samples since the technique is sensitive to both the nuclear and magnetic depth profiles. We note that the PNR and MOKE measurements were performed on samples with different CoFeB thicknesses (7 and 1.6 nm, respectively). In PNR, the thicker CoFeB allows for magnetic effects to be more prominently observed due to the additional reflectivity oscillations visible above the background. Since the temperature-dependent effects are observed in both CoFeB thicknesses, we expect observations to be similar for both sample sets. Further, we note that PNR is particularly sensitive to nitrogen movement from MnN into Ta since the scattering length density (SLD) of Mn is strongly negative while the SLD for nitrogen is strongly positive. Subsequently there is a large difference between the SLD of Ta (3.83×10^{-6} Å^{-2}) and TaN (6.89×10^{-6} Å^{-2}).

PNR for the R^{++} and R^{--} scattering cross sections are shown in Fig. 2 alongside theoretical fits; the magnetic contribution to the scattering is highlighted by the spin asymmetry (SA) in Supplemental Material Fig. 2, where SA = $(R^{++} - R^{--})/(R^{++} + R^{--})$. The PNR and SA show significant changes in key features as the annealing temperature

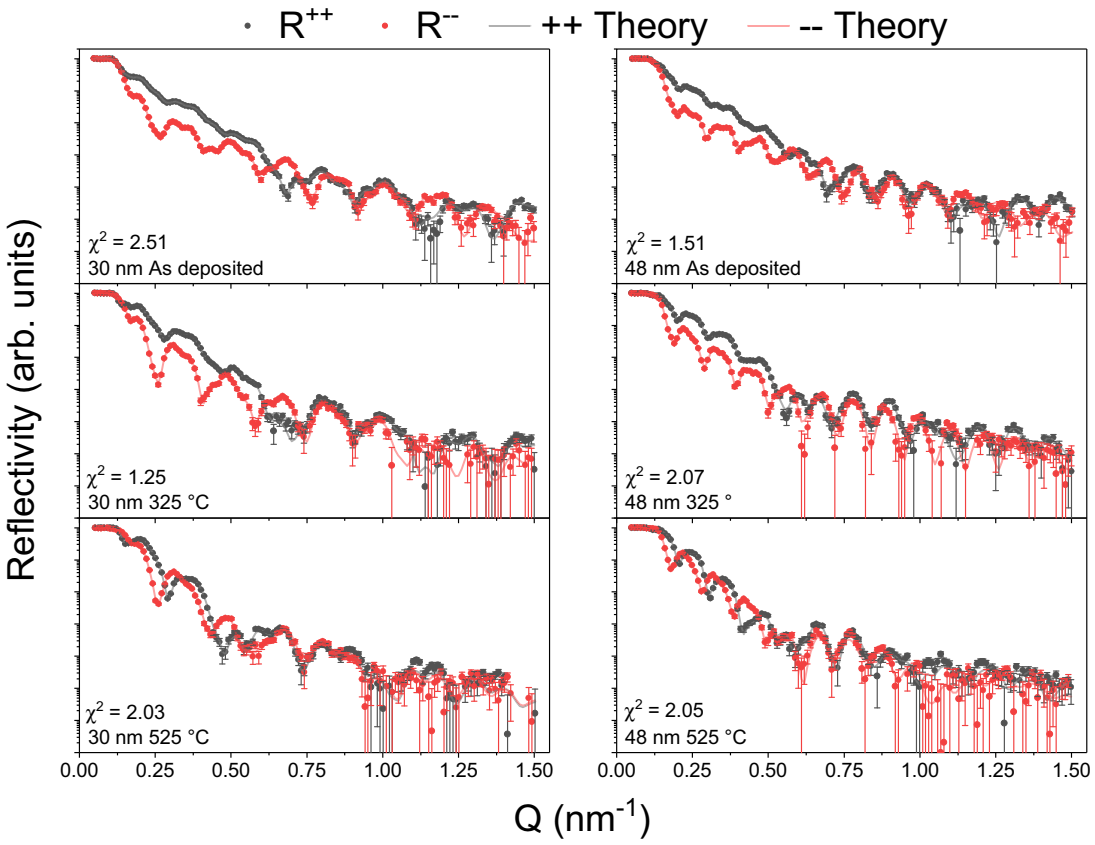

FIG. 2. Measured polarized neutron reflectivity (points) with theoretical fits (solid lines) in the non-spin-flip configuration. Results are shown for the 30 and 48 nm MnN in the as-deposited state, and after annealing at 325 and 525 °C. Error bars are representative of 1 σ.

is increased. The SLD profiles used to generate the theoretical fits can be seen in Figs. 3(a) and 3(b) for the nuclear structure and for the in-plane component of the magnetization as a function of depth. In this model, the MnN layer was divided into four regions, to allow for variation in the nitrogen content across the layer. Models including one, two, and three sublayers within the MnN layer were explored, and it was determined that four sublayers were required to yield a satisfactory χ^2 and nuclear scattering length density profiles that are physically meaningful. (An in-depth discussion of these simple models and resulting PNR fits can be found in the Supplemental Material [14].) The underlying Ta layer was separated into Ta and TaN regions since AES in prior work showed interdiffusion at the Ta and MnN interface. In the fitting of postannealed samples, a boron heavy layer was allowed to form at the CoFeB/TaO_x interface, as reported for CoFeB/Ta interfaces by Zhu *et al.* [17]. The Ta layer shows an initial TaN layer at the Ta/MnN interface, and the Ta absorbs more nitrogen as the annealing temperature increases until it is saturated at 525 °C. Fitting the PNR data at high annealing temperatures required profiles in which ferromagnetism sweeps into the top interface of the MnN layer, suggesting an intermixing of Mn with Fe or Co. While the peak magnetic SLD in the CoFeB decreases with increased annealing temperature, the total integrated magnetic SLD increases. The resulting PNR fits capture the resulting changes in the structural and magnetic depth profile extremely well, with a χ^2 of 2.51 or better.

In order to investigate the interfacial magnetic layer between CoFeB and MnN suggested by the PNR models, XMCD was employed on the 30 nm MnN with 7 nm CoFeB sample. XMCD for the L_2 and L_3 edges of Fe, Co, and Mn are shown in Fig. 4. The fine structure of the XAS shows a 2^+ Mn state due to the ionic bonding of Mn with N. We observe a dramatic change in the x-ray absorption L_3 edge intensities [Fig. 4(a)], for Co, Fe, and Mn, after annealing at 525 °C as compared to the preedge intensity—this normalization scheme provides the number of Fe, Co, and Mn atoms. Specifically, the Fe and Co signal decreases while the Mn signal dramatically increases. Since TEY-XMCD is sensitive primarily to the top 5 nm of the samples, this result provides insight into the interdiffusion process. The average x-ray absorption spectra, in Fig. 4(a), from measurements with antiparallel and parallel orientation of magnetization and photon helicity, are normalized by dividing the peak value by the preedge intensity to obtain the moment per atom [18]. The XMCD, in Figs. 4(b)–4(d), was normalized to the maximum intensity of the averaged XAS spectra and is shown as a percentage of the XAS intensity. By normalizing with this method, the XMCD signals can be directly compared; the magnitude of the XMCD for Fe [Fig. 4(b)] and Co [Fig. 4(c)] peaks increases with annealing temperature, which indicates the magnitude of magnetization increases [19]. In the case of Mn [Fig. 4(d)], there is a small (relative to that of Fe and Co) XMCD signal in the as-deposited sample. After annealing the samples at 325 and 525 °C, the Mn XMCD

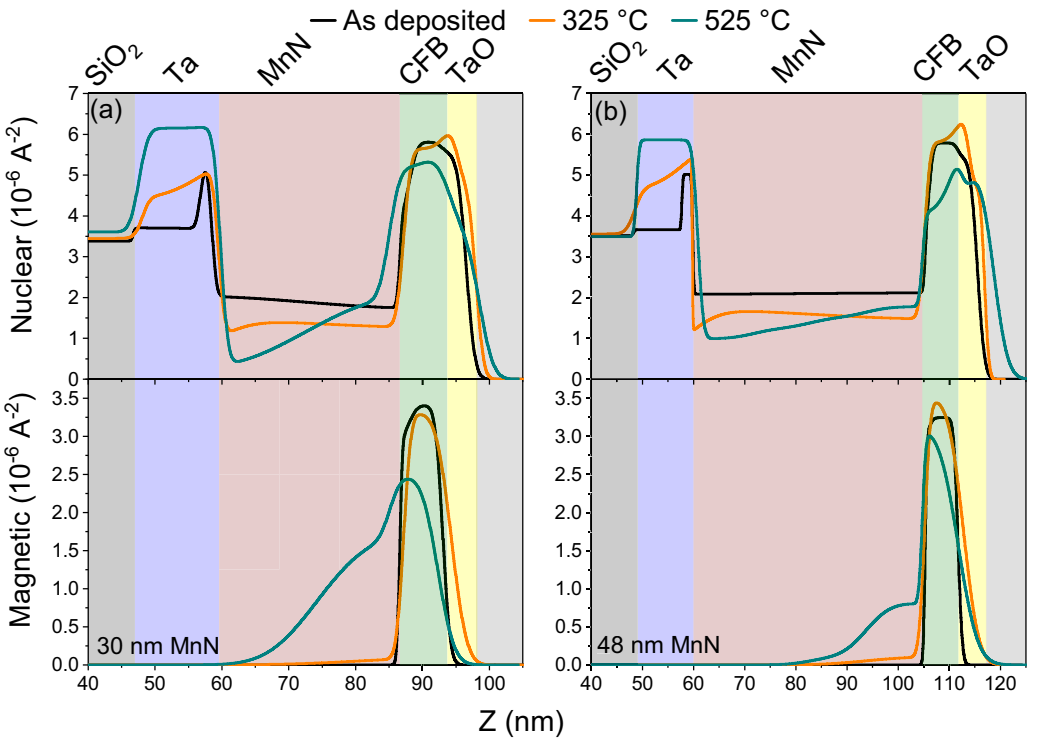

FIG. 3. Nuclear (top) and magnetic (bottom) scattering length density profiles for the 7 nm CoFeB samples with (a) 30- and (b) 48 nm of MnN. The layers are denoted by their nominal thicknesses and distance is referenced such that the substrate surface is at 0 nm.

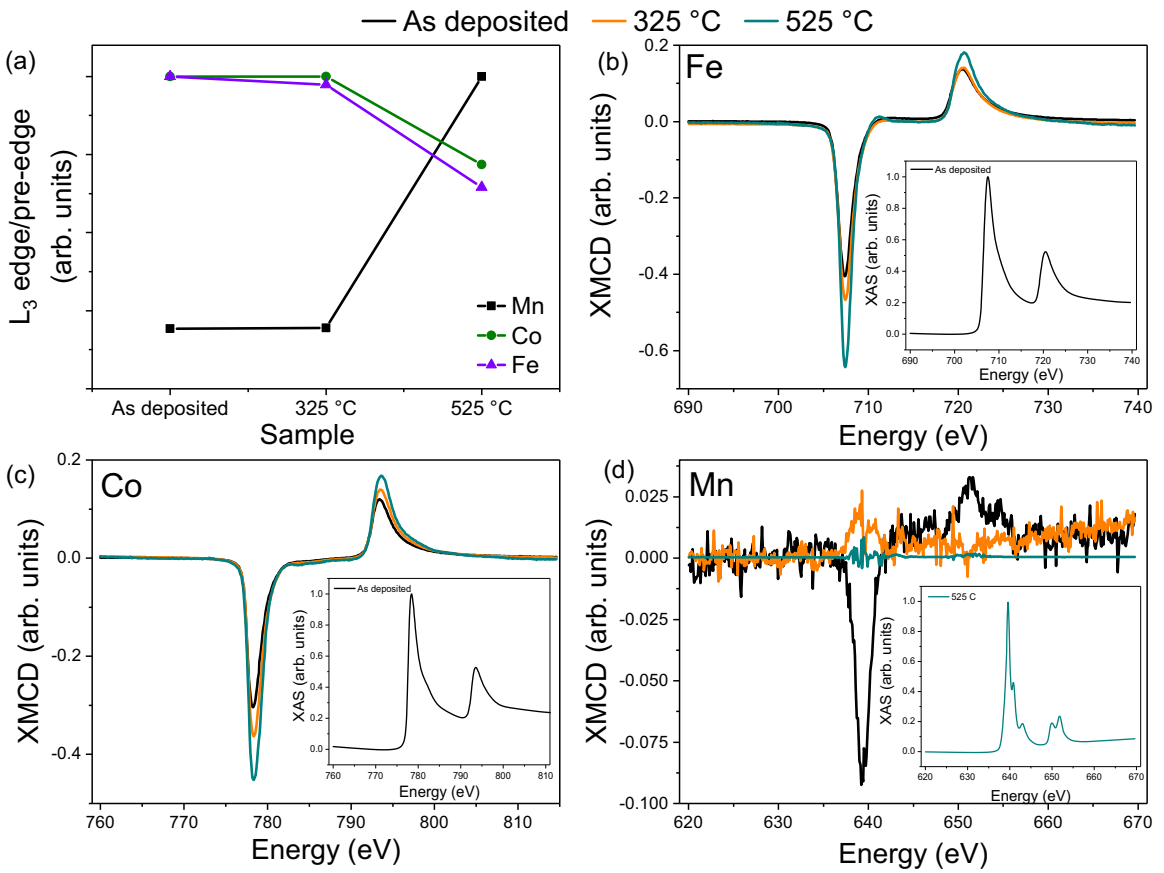

FIG. 4. XMCD and inset of XAS for (a) Fe, (b) Co, and (c) Mn with the XAS shown in the inset figures. (d) The L_3 peak intensity normalized to the preedge intensity as a function of annealing temperature. Data measured on the sample with 30 nm of MnN and 7 nm of CoFeB.

drops to zero. There is a small feature at the 325 °C Mn L_3 edge; however, due to how small the effect is, we cannot be certain the feature is significant and not caused by drift-related artifacts associated with the large intensity of the L_3 XAS edge. Furthermore, there is no definitive feature of opposite sign at the L_2 edge.

IV. DISCUSSION

From the PNR, XAS/XMCD, and XRD results, we can construct a comprehensive, element-specific understanding of why MnN thickness and field-annealing temperature have such strong effects on MnN-based exchange bias systems. Note that XRD, shown in Supplemental Material Fig. 1, further supports the structural changes observed with PNR and demonstrates that the samples studied in this work behave similarly to those in previous reports [8,20]. PNR reveals that the MnN layer is nitrogen rich in the as-deposited samples, which manifests through a nuclear SLD (2.09×10^{-6} Å^{-2}) larger than that of bulk MnN (1.77×10^{-6} Å^{-2}) and an expanded lattice observed by XRD (Supplemental Material Fig. 1 [14]). We also observe that the 30 nm MnN sample appears to have larger nitrogen content near the Ta interface than near the CoFeB interface, whereas this gradient for the as-deposited condition is not observed in the 48 nm sample (Supplemental Material Fig. 5). It remains unclear if this difference is intrinsically due to the MnN thickness or variations in the nitrogen reactive sputtering process. In the as-deposited state, XMCD reveals the presence of a small ferromagnetic moment on the Mn atoms [Fig. 4(d)], in comparison to the observed moments on Fe and Co, at the MnN/CoFeB interface, which is concluded to not be due to interdiffusion of Co or Fe into the MnN. Since the Mn moment in this thin layer is small and overshadowed by the strong neighboring ferromagnetic layer, it is challenging to resolve the magnetization of Mn, in proximity to a strong ferromagnet like CoFeB, with PNR modeling. XMCD shows that the moment on the Mn quickly disappears after annealing, as the antiferromagnetic θ phase is stabilized into the bulk crystal structure. At the Ta/MnN interface there is an intermediate TaN layer, even in the as-deposited state, which is probably created by the reactive plasma exposition during the growth process. After annealing at 325 °C, nitrogen migrates from the MnN layer into the underlying Ta layer, which leads to a gradient in nitrogen content across the Ta and MnN layers. This nitrogen migration, which occurs in a similar fashion for both the 30 and 48 nm MnN samples, causes the average nuclear SLD in the MnN and Ta layers to decrease and increase, respectively. At this field-annealing condition, a high nuclear SLD region at the top of the CoFeB arises, which a previous PNR report by Zhu *et al.* concluded was due to boron segregating out of the film [17]. Note that later electron microscopy studies by Wang *et al.* suggest the B moved into interstitial sites of neighboring TaO_x layers [21]. This boron segregation is expected to yield an increased magnetization in the remaining CoFe film, as was confirmed by an increase in the XMCD signal for both Fe and Co $L_{2,3}$ edges. While the magnetic scattering length density peak value obtained from PNR decreases as the annealing temperature increases, the overall integrated magnetic SLD (which is magnetization per depth) increases due to the migration of Fe and Co. Thus, the changes in magnetic scattering length density are consistent with the increase in XMCD signal, which measures magnetic moment per atom.

Increasing the field-annealing temperature to 525 °C leads to dramatic differences between the 30 and 48 nm MnN samples in the MOKE hysteresis loops [Fig. 1(a)], SLD profiles (Fig. 3), and XMCD spectra [Figs. 4(b)–4(d)]. In both samples, we observe that the Ta becomes almost entirely saturated with nitrogen absorbed from the MnN layer, as shown by an increase in the SLD in the Ta layer which approaches the bulk TaN value (6.8×10^{-6} Å^{-2}). The removal of N from MnN results in intermixing of Mn with Fe and Co at the MnN/CoFeB interface; Mn in the nominal CoFeB causes the nuclear SLD to decrease, whereas Co and Fe in the MnN layer results in an increased nuclear SLD. We clearly see in the magnetic SLD profile that this interdiffusion also leads to ferromagnetism sweeping into the MnN layer, which is attributed to the intermixing of Mn with Fe and Co since the SLD near the top of the nominal MnN layer increases. However, we cannot rule out the formation of iron- and cobalt nitrides, both of which have ferromagnetic and antiferromagnetic phases [22,23]. As the 30 nm MnN layer contains less nitrogen to donate, the resulting nuclear SLD gradient in MnN is far more extreme than in the case of 48 nm MnN. We postulate that the more extreme case of nitrogen deficiency yields more vacancies that aid interdiffusion, so that intermixing is significantly more pronounced in the 30 nm sample—shown in both the nuclear and magnetic SLD profiles with the latter extending through most of the nominal MnN layer [Fig. 3(a)]. The XAS intensity [Fig. 4(a)] also supports a picture of interdiffusion at the MnN/CoFeB interface after high-temperature annealing. The intensity of the L_3 edge for Fe, Co, and Mn is the same for the as-deposited and 325 °C annealing condition, but exhibits a sharp increase in the Mn signal and decrease for Fe and Co. Since we collected the XAS and XMCD in TEY mode, the data are primarily sensitive to the surface with signal contributions originating deeper in the film being attenuated with a characteristic decay length of 5 nm. We therefore conclude that the Fe and Co diffused deeper into the sample, while the Mn migrated towards the surface, in excellent agreement with the SLD profiles.

The MOKE measurements show that the exchange bias is progressively enhanced by increased annealing temperature for the sample with 48 nm of MnN, but the exchange bias disappears at high annealing temperature when the MnN thickness is 30 nm. We surmise that the 30 nm MnN layer becomes so nitrogen deficient that the layer is no longer antiferromagnetic after the high-temperature annealing process. Since the exchange bias also disappears in the 1.6 nm CoFeB sample, we conclude that interdiffusion of Co, Fe, and Mn is not the cause because the intermixing will be far more limited than in the 7 nm CoFeB samples. However, in the 48 nm MnN sample, there is enough nitrogen remaining after the Ta layer becomes saturated with nitrogen to maintain θ-phase MnN which preserves the antiferromagnet/ferromagnet interface. Furthermore, we observe that the thicker MnN sample displays an increased exchange bias field (Supplemental Material Fig. 2) even upon annealing at 525 °C. XRD

measurements (Supplemental Material Fig. 1) conclusively demonstrated that the increased annealing temperature allows for the remaining MnN to relax into the bulk crystal structure with improved texture, which likely accounts for the enhanced exchange bias field. However, additional studies to better understand the role that intermixing between Co, Fe, and Mn has on the magnetic properties are of interest. A thinner Ta layer may allow for thin MnN to maintain the exchange bias effect after high-temperature annealing since less nitrogen will be required to saturate the layer. Alternatively, preemptively nitriding the Ta layer during deposition or including a diffusion barrier may also improve the thermal stability of MnN/CoFeB systems to realize even larger bias fields.

V. CONCLUSIONS

In this work, we resolve the question of thickness- and annealing-temperature-dependent exchange bias effect in MnN/CoFeB heterostructures. PNR, XMCD, and XRD characterization have been used to probe both the nuclear and magnetic structure to understand the role of nitrogen diffusion in MnN-based systems. We have shown that nitrogen migrates from the initially nitrogen-heavy MnN films into a neighboring Ta layer as a function of annealing temperature. When there is not an adequate amount of nitrogen to maintain the stability of the entire MnN film, then Co and Fe begin to diffuse into the nominal MnN layer, which can decrease, or even eliminate, the exchange bias. An increase in the net magnetization of the ferromagnetic layer at high annealing temperatures has also been observed, which is attributed to both the segregation of boron to the top interface and intermixing with the underlying Mn heavy layer. The inclusion of a diffusion barrier layer at the Ta/MnN interface, such as TaN, or a thinner seed layer may allow for higher annealing temperatures to be used without degrading the MnN layer, opening the possibility of even larger exchange bias fields in MnN-based MTJs.

ACKNOWLEDGMENTS

P.Q. acknowledges support from the National Research Council Research Associateship Program. Research performed in part at the NIST Center for Nanoscale Science and Technology. This research used resources of the Advanced Light Source, which is a DOE Office of Science User Facility under Contract No. DE-AC02-05CH11231. M.M. acknowledges financial support from the Deutsche Forschungsgemeinschaft (DFG) under Sign No. ME 4389/2-1.

[1] A. V. Khvalkovskiy, D. Apalkov, S. Watts, R. Chepulskii, R. S. Beach, A. Ong, X. Tang, A. Driskill-Smith, W. H. Butler, P. B. Visscher, D. Lottis, E. Chen, V. Nikitin, and M. Krounbi, J. Phys. D: Appl. Phys. **46**, 139601 (2013).

[2] K. L. Wang, J. G. Alzate, and P. Khalili Amiri, J. Phys. D **46**, 074003 (2013).

[3] A. Makarov, T. Windbacher, V. Sverdlov, and S. Selberherr, Semicond. Sci. Technol. **31**, 113006 (2016).

[4] T. Endoh, H. Koike, S. Ikeda, T. Hanyu, and H. Ohno, IEEE J. Emerging Sel. Top. Circuits Syst. **6**, 109 (2016).

[5] J. Nogues and I. K. Schuller, J. Magn. Magn. Mater. **192**, 203 (1999).

[6] M. Meinert, B. Büker, D. Graulich, and M. Dunz, Phys. Rev. B **92**, 144408 (2015).

[7] P. Zilske, D. Graulich, M. Dunz, and M. Meinert, Appl. Phys. Lett. **110**, 192402 (2017).

[8] M. Dunz, J. Schmalhorst, and M. Meinert, AIP Adv. **8**, 056304 (2018).

[9] Y. Ferrante, J. Jeong, R. Saha, S. V. Faleev, M. G. Samant, T. Topuria, H. Deniz, and S. S. P. Parkin, APL Mater. **7**, 031103 (2019).

[10] N. A. Gokcen, Alloy Phase Diagrams **11**, 33 (1990).

[11] K. Suzuki, T. Kaneko, H. Yoshida, Y. Obi, H. Fujimori, and H. Morita, J. Alloys Compd. **306**, 66 (2000).

[12] M. Tabuchi, M. Takahashi, and F. Kanamaru, J. Alloys Compd. **210**, 143 (1994).

[13] K. Suzuki, Y. Yamaguchi, T. Kaneko, H. Yoshida, Y. Obi, H. Fujimori, and H. Morita, J. Phys. Soc. Jpn. **70**, 1084 (2001).

[14] See Supplemental Material at http://link.aps.org/supplemental/10.1103/PhysRevMaterials.3.064413 for XRD characterization and additional analysis of the PNR and modeling. Alternative models with fewer MnN sublayers are shown.

[15] B. J. Kirby, P. A. Kienzle, B. B. Maranville, N. F. Berk, J. Krycka, F. Heinrich, and C. F. Majkrzak, Curr. Opin. Colloid Interface Sci. **17**, 44 (2012).

[16] P. A. Kienzle, B. B. Maranville, K. V. O'Donovan, J. F. Ankner, N. F. Berk, and C. F. Majkrzak, https://www.nist.gov/ncnr/reflectometry-software, 2017.

[17] T. Zhu, Y. Yang, R. C. Yu, H. Ambaye, V. Lauter, and J. Q. Xiao, Appl. Phys. Lett. **100**, 202406 (2012).

[18] W. L. O'Brien and B. P. Tonner, Phys. Rev. B **50**, 12672 (1994).

[19] C. Piamonteze, P. Miedema, and F. M. F. de Groot, Phys. Rev. B **80**, 184410 (2009).

[20] M. Dunz, B. Büker, and M. Meinert, J. Appl. Phys. **124**, 203902 (2018).

[21] Z. Wang, M. Saito, K. P. McKenna, S. Fukami, H. Sato, S. Ikeda, H. Ohno, and Y. Ikuhara, Nano Lett. **16**, 1530 (2016).

[22] J. M. D. Coey and P. A. I. Smith, J. Magn. Magn. Mater. **200**, 405 (1999).

[23] M. B. Lourenço, M. D. Carvalho, P. Fonseca, T. Gasche, G. Evans, M. Godinho, and M. M. Cruz, J. Alloys Compd. **612**, 176 (2014).